Turbulence Measurements for Heated Gas Slot Injection in Supersonic Flow

C. R. Hyde,* B. R. Smith,* J. A. Schetz,† and D. A. Walker‡
Virginia Polytechnic Institute and State University, Blacksburg, Virginia 24061

This paper presents mean and turbulence profile measurements in the flow created by supersonic, tangential injection of heated air into a supersonic air flow. Spark-Schlieren and Nanosecond Shadowgraph photographs give qualitative and some quantitative descriptions of the resulting flow. The profile measurements were made at four axial stations ($x/H = 0.25$, 4, 10, and 20). Tests were also conducted to study the influence of an oblique wave ($P_2/P_1 \sim 1.8$) impinging on the shear layer between stations 3 and 4. All of the results are compared with results for unheated injection at the same conditions. Mean flow quantities are surveyed by a pitot tube, a cone-static probe, and a diffuser thermocouple probe. Fluctuations are measured by hot-wire anemometer. The mean flow and turbulence measurements are also combined to deduce Favre-averaged velocity fluctuations, u''. The freestream Mach number was $M_\infty = 3$ with $P_{t\infty} = 6.5$ atm and $T_{t\infty} = 300$ K giving a freestream $Re = 2 \times 10^6$/cm. The slot Mach number was $M_j = 1.7$ with $P_{tj} = 0.73$ atm and $T_{tj} = 420$ K. All of this produces a density ratio of $\rho_j/\rho_\infty = 0.3$ and a velocity ratio of $u_j/u_\infty = 0.9$. The slot height was 1.2 cm, and the air-side boundary layer was 0.7 cm. The heated slot flow did not create a marked difference in the location of the merging of the freestream boundary layer with the slot flow when compared to the unheated slot flow. Some increases in the absolute turbulence levels were seen in the heated flow, and the location of the maximum turbulence shifted. Heating enhanced the mixing in the shear layer and in the injected flow by the last station. Shock interaction with the shear layer generally resulted in elevated conventional turbulence and had little effect on u''.

Nomenclature

H = slot height
ℓ/d = length to diameter ratio of wire
m = mass flux, ρu
M = Mach number
P_t = pressure
Re = Reynolds number
T_t = total temperature
u,v = axial and transverse velocity components
x,y = Cartesian coordinate system
δ = boundary-layer thickness
ρ = local density
Θ = $(T_t - T_{t\infty})/(T_{tj} - T_{t\infty})$

Subscripts

j = injectant or jet
t = total condition
∞ = freestream condition
1 = ahead of shock
2 = after shock

Superscripts

$(\,)'$ = root-mean-square turbulent quantity
$\overline{(\,)}''$ = Favre-averaged quantity
$(\bar{\ })$ = Reynolds-averaged mean value

Received June 29, 1989; revision received Nov. 3, 1989.

*Graduate Assistant, Aerospace and Ocean Engineering Department. Student Member AIAA.

†W. Martin Johnson Professor and Department Head, Aerospace and Ocean Engineering Department. Fellow AIAA.

‡Assistant Professor, Aerospace and Ocean Engineering Department. Member AIAA.

Introduction

RECENT interest in hypersonic vehicles has revealed a need for increased research on turbulent mixing in high-speed flows. Much experimental hypersonic research is aimed at thorough studies of idealized benchmark test configurations to produce a data base for computer modeling and to obtain information useful in specific applications. A study of slot injection of a supersonic secondary stream into a parallel supersonic primary flow is useful in both respects. This flow is of possible interest in fuel injection, surface cooling, skin friction reduction, and/or energy addition to the boundary layer to prevent separation. Injection from a rearward-facing step also enhances transition, and transition is expected to be a problem at high altitude. In the case of tangential fuel injection, thrust is derived from the fuel, the surface is cooled, and skin friction is reduced.

A selection of related past work with supersonic flow is in Refs. 1–13. Other relevant studies have been concerned with supersonic "free" shear layers where the mixing layer is distant from any wall. But, studies in which both mean and turbulence measurements have been made are rare. Turbulence measurements, however, are crucial in improving turbulence models used in computer simulations of supersonic flow. There is interest in both Reynolds-averaged turbulence quantities (e.g., $\overline{u'^2}$) and Favre-averaged turbulence quantities (e.g., u'') for both flow physics understanding and turbulence modeling. Little or no Favre-averaged data for supersonic flows is available. Laser Doppler velocimetry (LDV) and hot-wire anemometry can both measure turbulence in supersonic flows.[14–18] Our studies used advanced hot-wire methods to avoid seeding.

Hot wires respond to changes in flow density, velocity, and total temperature. For high Reynolds number flows with Mach numbers from 1.2 to 5, hot-wire sensitivities to ρ and u are essentially equal and independent of M so that the wire response can be resolved into ρu and T_t fluctuations.[16,17,18] Without other information or simplifying assumptions, ρ and u cannot be separated. Two unknowns require multiple measurements. One method uses two very closely spaced wires

operating simultaneously at different overheats. The method used here has one wire operating at several temperatures cycled quickly. Redundancy of overheats allows a least-squares analysis.

The current study models, in a basic research sense, a SCRAMjet combustor. It consists of a Mach 1.7 air stream injected parallel to a Mach 3 air freestream. This freestream Mach number is a typical value for a combustor at flight Mach numbers near 8. Freestream total pressure and temperature were 6.5 atm and 300 K, respectively. The thick (0.7 cm), initial boundary layer chosen is consistent with an aircraft whose forebody is used for early flow compression. The slot height (1.2 cm) was of the order of the boundary thickness, $\delta_i/H = 0.6$. The secondary flow temperature was varied from 300 to 420 K to test the effects of density and velocity ratio changes. Measurements were also taken to determine the effect of weak shock ($P_2/P_1 = 1.8$) impingement on the shear layer.

Mean and turbulent quantities were measured using pitot, cone-static, diffuser thermocouple and hot-wire probes. Computer-controlled instrumentation greatly improved the amount and quality of the data taken. In addition, Spark Schlieren photographs and Nanosecond Shadowgraphs were taken to aid interpretation of results and to allow measurement of prominent flow features.

Apparatus and Methods

Facilities

The data was obtained in the 23 × 23 cm blowdown supersonic wind tunnel at Virginia Tech, which provided run times of about 10 s at a Mach number of 3. The resulting freestream Reynolds number is 2×10^6/cm. The test section was 11.4 cm high, 22.8 cm wide, and more than 30 cm in length in the streamwise direction.

Slot Model

The slot injection model was built into the wind-tunnel nozzle as shown in Fig. 1. The supersonic tangential injector consisted of a 1.21-cm high, downstream facing slot injector separated from the Mach 3 mainstream by a splitter plate 0.5 mm thick. The contoured, converging-diverging injector had an area ratio of 1.55, and it was run with a total pressure of 0.73 atm, which gave a nominal slot Mach number of 1.7.

For the heated injected case, a nickel tube heater was used. Injection temperature could be controlled to within ±5 K.

The test section wall was constructed of stainless steel, and the temperature of the wall was not controlled.

Measurement Stations

Profiles across the shear layer were measured and recorded at four stations. Station 1, at $x/H = 0.25$, is an initial value region. At $x/H = 4$, station 2 provides data for the beginning of the development of the shear layer. All waves have left the mixing region by this station. At $x/H = 10$ (station 3), the shear layer has developed substantially. Station 4, at $x/H = 20$, provides data for a developed region as the wall boundary layer has merged with the shear layer.

Mean Flow Measurements

The cone-static probe consists of a 10-deg semivertex angle cone of base diameter 1.6 mm. The pitot probe is a simple flat-faced tube. A ceramic tipped, vented, diffuser-type thermocouple probe was used to measure the total temperature. The sampling area of the probes was about 1 × 1 mm.

A computer-controlled probe transverse system allowed data measurements up to heights of $y/H = 3.5$ at a rate of 0.5 cm/s.

Hot-Wire Probe

The hot-wire probe used is a straight wire with a length of 1.25 mm and a diameter of 5 μm, giving an ℓ/d ratio of 250. The constant-temperature hot-wire circuit was designed by Walker et al.[19] to step the hot-wire through eight temperatures in quick succession, each temperature lasting 10 ms. A final 10 ms delay after the last temperature allowed the wire to reach thermal equilibrium at the lowest overheat at the next vertical position. Ten milliseconds is on the order of 1000 integral times, so taking fewer than 1000 samples assures that each sample is independent of the previous one.

Data Acquisition System

A personal computer (PC) equipped with a high-speed A/D board is the primary source of acquiring data. The A/D board has a maximum of 16 channels and samples 12 bits at a maximum rate of 100 kHz. The main use of the A/D board is to convert pressure, temperature, and Linear Voltage Displacement Transformer (LVDT) signals from analog to digital. An additional virtue of the A/D board is its digital output for relay switching, which is used for starting and stopping the tunnel as well as controlling the position of the probe by switching a voltage to the traverse motor. Another quality of the A/D board is its ability to produce analog output for pressure control.

Data Reduction Procedure

The ratio p_c/p_{t2} was used to determine local Mach number. That was used with the measured $\bar{T}_t$ to obtain $\bar{T}$ and thus $\bar{a}$

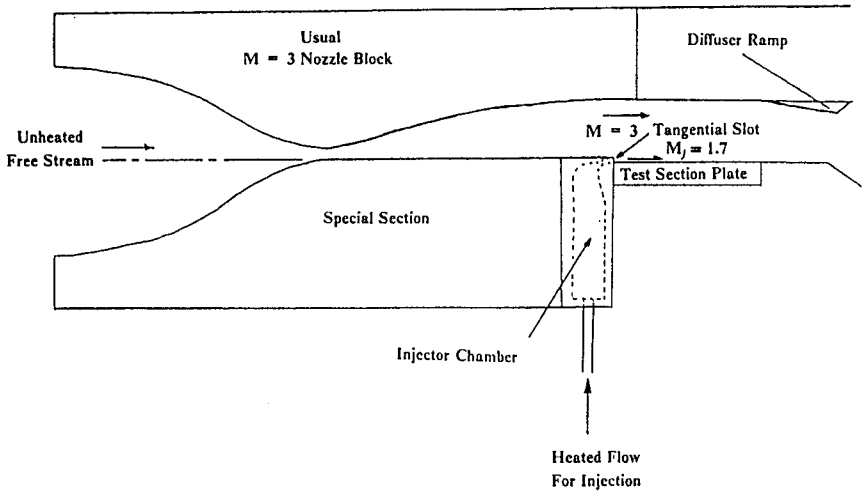

Fig. 1 Schematic of the slot injection test configuration.

and $\bar{u}$. Finally, Mach number and P_c were used to obtain $\bar{P}$, and $\bar{P}$ and $\bar{T}$ produced $\bar{\rho}$.

At each of the four streamwise stations, measurements were taken at 105 vertical positions above the lower wall. During each run, turbulence was measured at 35 positions, one-third of an entire profile. There was a small vertical overlap of 0.6 mm between runs. The T_{t_∞}, the p_{t_∞}, and the LVDT were sampled simultaneously at 2 kHz with 16 samples of each taken at each location.

The derivation of the hot-wire reduction method can be found in Walker et al.[19] At each height, data were taken at as many as eight distinct overheats. At each overheat, 160 samples were taken, i.e., 1280 samples/position. During analysis, the first and last samples were dropped as just discussed. In addition, the largest and smallest samples were removed to eliminate possible spurious data caused by oil droplet impact on the wire. Averages, mean square values, and variances were calculated using all remaining samples.

When the turbulence levels were small, scatter in the data occasionally resulted in negative values for some of the computed mean square quantities, especially in T_t'. These were removed before rms values were computed. The rms values were then spatially filtered by a five-point binomial filter. Although smoothing in this way can introduce spatial aliasing into the profiles, it was judged necessary due to the scatter which resulted from the limited number of samples at each point.

The hot-wire methods just described yield $\overline{\rho u}$, $\overline{(\rho u)'^2}$, $\bar{T}_t$, and $\overline{T_t'^2}$. Mean-flow probe methods such as used here yield some type of mean quantities. The matter is complex and not subject to direct analysis because each probe (e.g., a pitot probe) measures a kind of mean quantity, and then the results from several probes (pitot, one-static and total temperature) are combined to infer "mean" values of Mach number, velocity, density, etc. We are assuming here that our mean-flow methods yield Reynolds-averaged mean quantities, i.e., $\bar{M}$, $\bar{\rho}$, $\bar{u}$, etc. If such probes yielded Favre-averaged mean quantities, the $\overline{\rho u}$ result would be the same as from the hot-wire probes, and the results to be presented later show that such is not the case. With these assumptions, the $\overline{\rho u}$ hot-wire results and the mean-flow results for $\bar{\rho}$ and $\bar{u}$ can be used to deduce $\overline{u''}$ from

$$\frac{\overline{u''}}{\bar{u}} = 1 - \frac{\overline{\rho u}}{\bar{\rho} \cdot \bar{u}}$$

Results and Discussion

Flow Visualization

Spark Schlieren photographs (10^{-6} s) of both the unheated and heated injection flowfields without shock impingement are presented in Figs. 2 and 3. The flow is from left to right, and the backward-facing step in the wall contour is evident at the lower left. The turbulent boundary layer approaching the slot is shown. The photograph also shows that the injected flow was slightly overexpanded so that the shear layer deflects towards the wall initially. The adjustment shock and its reflection in the injectant stream are visible just downstream of the slot. The "lip" shock characteristic of base flows can be seen propagating up into the freestream.

Looking at the unheated slot injection schlieren first, the progression of the shear-layer development is evident. The four measurement stations were located to capture four distinct regions of the shear layer. Station 1 includes many waves in both the slot and the mainstream boundary layer. At station 2, the slot flow is not merged with the freestream

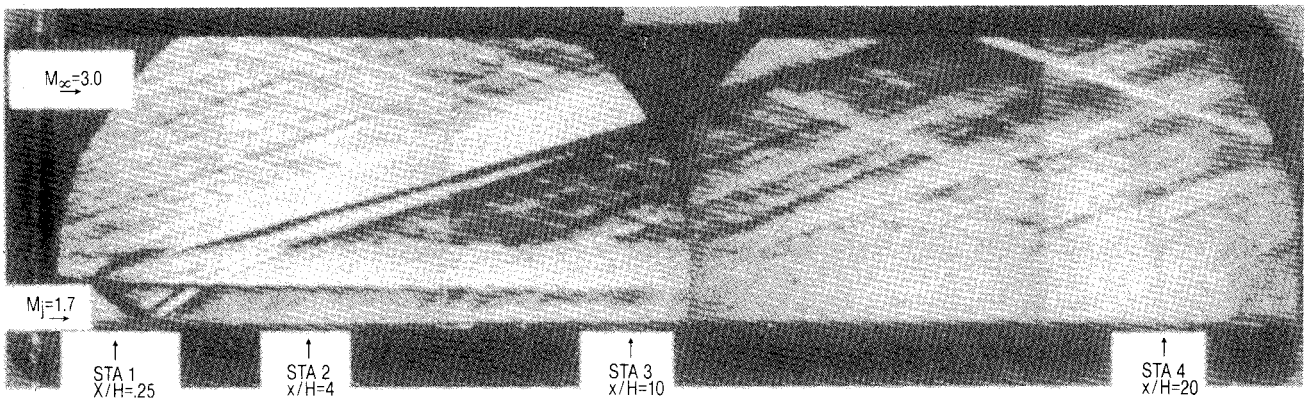

Fig. 2 Spark (10^{-6} s) schlieren of unheated ($T_{tj} = 300$ K), $M_j = 1.7$ slot injection into a $M_1 = 3$ stream.

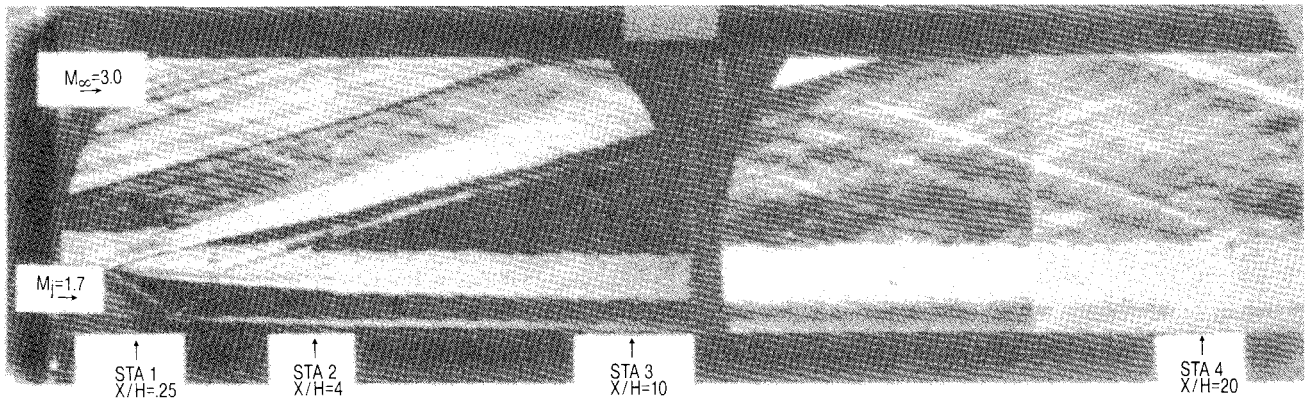

Fig. 3 Spark (10^{-6} s) schlieren of heated ($T_{tj} = 420$ K), $M_j = 1.7$ slot injection into a $M_1 = 3$ stream.

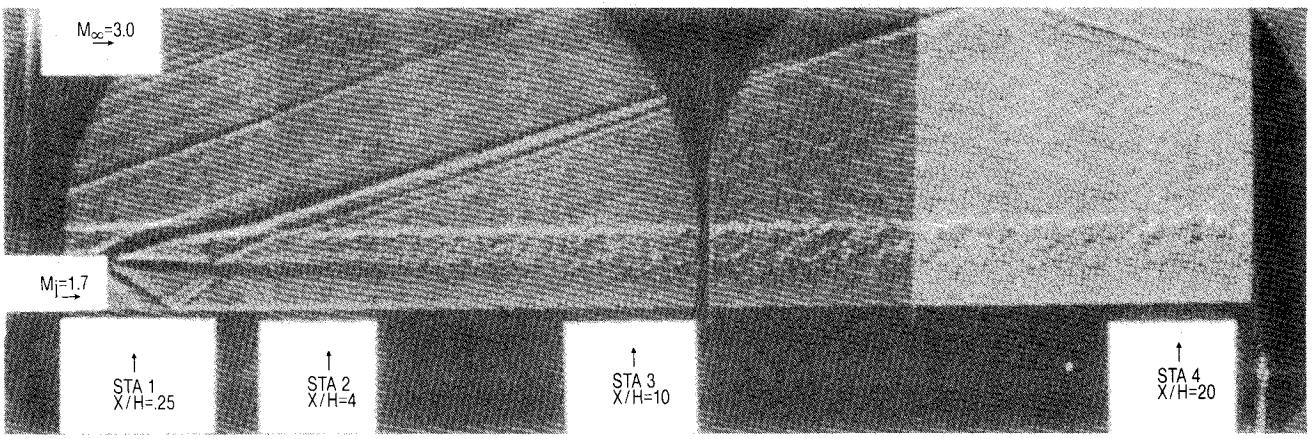

Fig. 4 Nano (10^{-8} s) shadowgraph of heated ($T_{tj} = 420$ K), $M_j = 1.7$ slot injection into a $M_1 = 3$ stream.

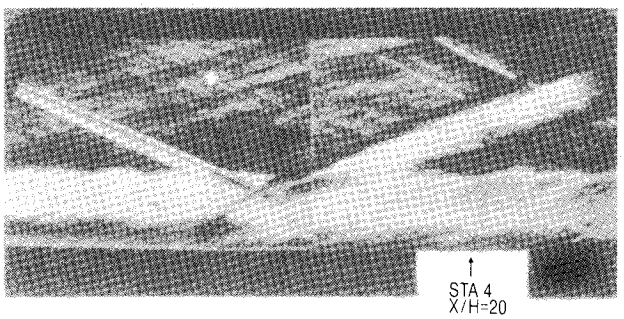

Fig. 5 Spark (10^{-6} s) schlieren of shock-wave impingement.

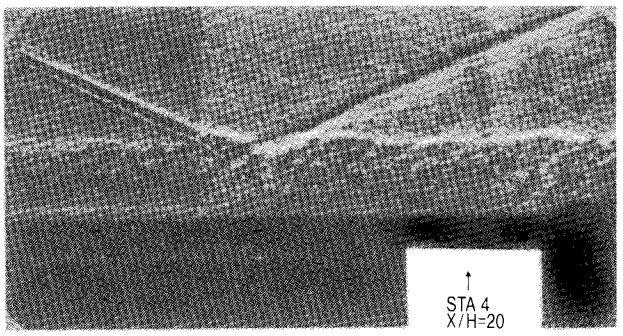

Fig. 6 Nano (10^{-8} s) shadowgraph of shock-wave impingement.

boundary layer so that it also provides an "initial condition" type flowfield. The station 2 shear flow region is free of the shocks emanating from the splitter plate. Some mixing occurs by station 3, but the slot potential core still remains. At station 4, most of the potential core slot flow has disappeared.

The overall flowfield features of the heated slot injection case are qualitatively similar to those in the unheated case; though the heated slot mass flow is approximately 15% less. The schlieren of the heated slot flowfield shows some detailed differences. First, due to the larger density gradients, a lighter white streak appears leaving the splitter plate beneath the boundary layer. Second, the pressure adjustments, resulting from the shocks and expansions off the splitter plate, are slightly different. Third, the potential core appears longer for the heated case, but no measurable differences in the sizes of the shear-layer features are evident when comparing the schlierens. Last, the heated injection flow schlieren shows an extra weak oblique shock emanating from the upstream nozzle block, which originates at a slightly misaligned junction in the wall upstream of the slot injection station and affects only the primary flow.

Some turbulence information can also be obtained from the schlieren photos. Clearly seen are the low-energy acoustics in the freestream, probably a significant part of the $(\rho u)'$ later measured there. More detail is available in the shorter duration (10^{-8} s) Nanosecond Shadowgraph in Fig. 4. The scale of the largest visible turbulent structures in the shear layer of the heated case was on the order of one-third of its thickness. They appear about twice as large as and better defined than were found for the unheated case. The increased structure size is an indication of the entrainment of large pockets of low-density gas into the lower-temperature shear layer. The large-scale structure angle in both cases appears about 50 deg.

Figures 5 and 6 are a Spark Schlieren photograph and a Nanosecond Shadowgraph of the shock impingement upstream of the last station caused by a wedge on the tunnel wall. They show the incident shock reflecting off of the top of the shear layer. A weak shock also penetrates into the shear layer, but it is dissipated as it approaches the subsonic flow near the wall. The adverse pressure gradient produced creates an increase in the shear/boundary layer thickness of approximately 10%. The Nanosecond Shadowgraph indicates an increased turbulence level after the interaction.

Mean Flow Profiles

Because of the weak shock from the upstream nozzle block, which was seen in the photographs, the heated profiles have some small differences from the unheated profiles as the freestream is approached. Also, some measurement problems were experienced at station 1 in the complex region just downstream of the slot lip where there are very large transverse gradients and closely spaced weak shocks (see Fig. 2). Our "small" probes were nonetheless apparently too large. For that reason, detailed results will only be given here for stations 2, 3, and 4. Also, due to space limitation, only profiles of $\bar{u}$, $\bar{T}_t$, and $\bar{\rho}$ will be shown. Profiles of $\bar{M}$ and $(\overline{\rho u})$ are also available to the interested reader.

The velocity profiles are shown in Fig. 7 for the cases without shock impingement. As expected, the injected velocities are greater for the heated flow than for the unheated flow in the slot. Accordingly, the heated slot case produces a smaller velocity gradient $(\bar{u}_\infty - \bar{u}_j)/H$ than the unheated slot case, so the heated slot flow should not tend to mix as quickly with the main flow as the unheated slot flow based on simple turbulent exchange models. Station 3 profiles show the largest difference between the unheated and heated velocity profile mixing. At station 3, the unheated case, which has a larger velocity gradient, does not show as pronounced a core flow as the heated case. This suggests that the unheated velocity profile is mixing out slightly faster. Nonetheless, at station 4,

the heated and unheated injection velocity profiles are nearly identical for the whole traverse. The Mach number and other profiles are not identical.

Figure 8 shows nondimensionalized total temperature profiles for the heated flow. The profile at station 2 shows a maximum near the top of the slot flow, which may indicate a small temperature nonuniformity in the slot exit flow. The profiles show a continually diminishing size of the potential core as the flow progresses downstream. Station 1 had a heated core up to approximately 0.8 slot heights, whereas stations 2, 3, and 4 only show excess heat up to 0.75, 0.65, and 0.45 slot heights, respectively. By station 4, the maximum value of the temperature is reduced approximately 20%.

As the velocity in the slot increases with temperature, the density in the slot decreases resulting in $(\rho_j/\rho_\infty)_{\text{hot}} \sim 0.32$ and $(\rho_j/\rho_\infty)_{\text{cold}} \sim 0.45$. The density profiles are given in Fig. 9. Because substantial mixing has occurred by station 4, the heated flow density profile is closer to the unheated flow density profile at this station. Since the density gradient produced by the heated injection flow is greater, the heated flow density profiles may tend to mix quicker because of the density instabilities induced by the larger gradients. Of course, this effect cannot be separated from the important preceding velocity gradient effects. At station 3, the potential core for the heated injection is not as pronounced as the core flow density for the unheated flow. The top of the potential core

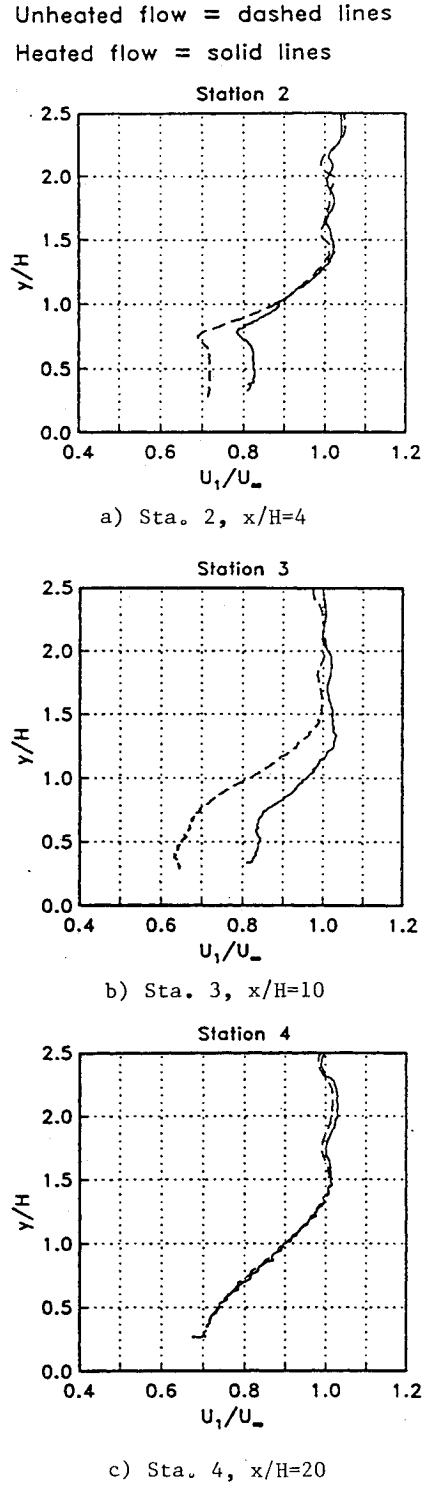

Fig. 7 Mean velocity profiles.

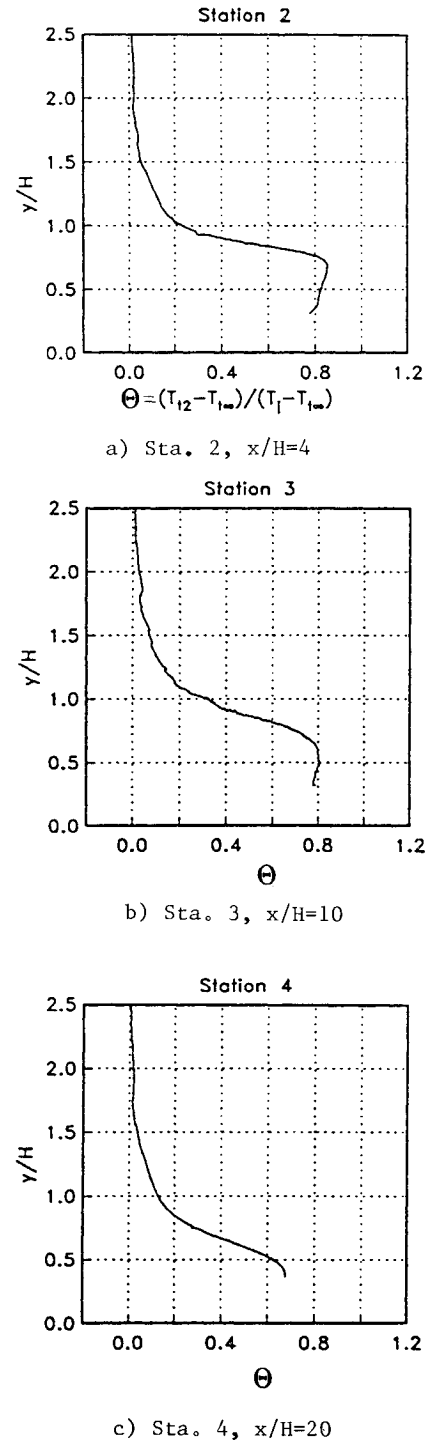

Fig. 8 Mean total temperature profiles.

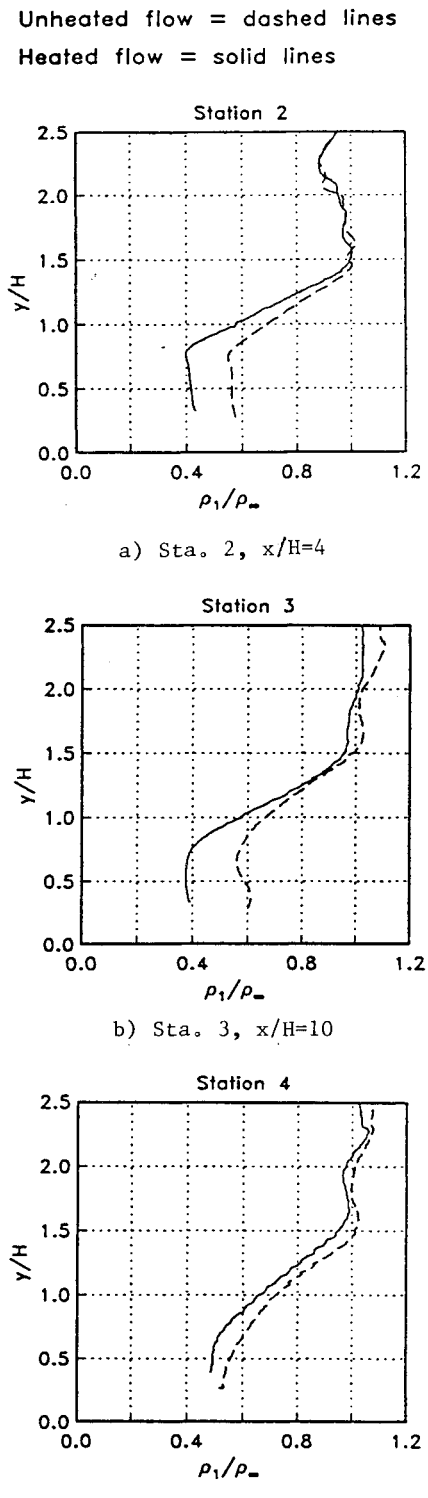

Fig. 9 Mean density profiles.

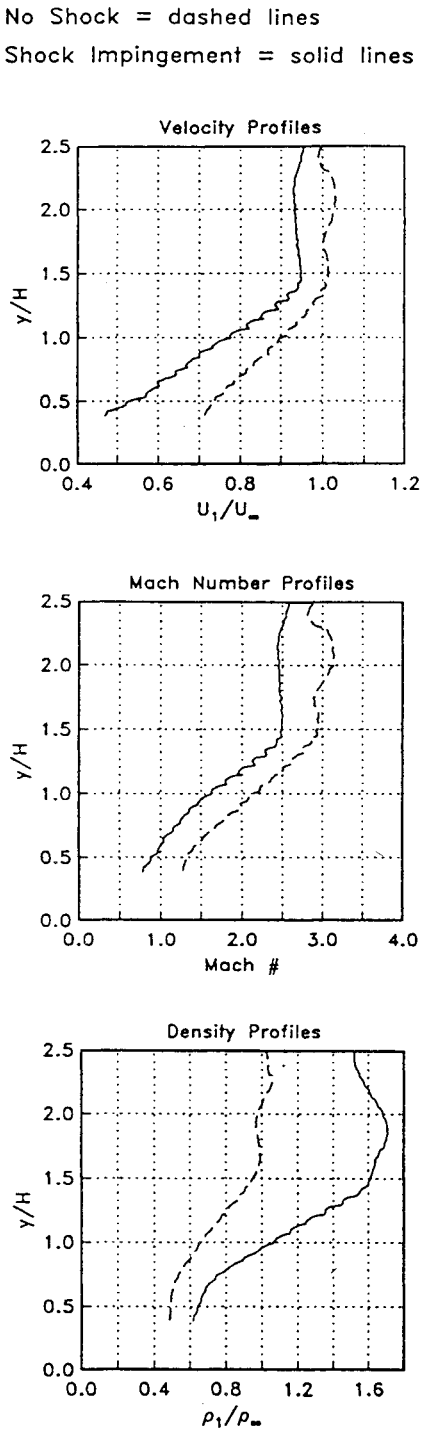

Fig. 10 Mean profiles at station 4, $x/H = 20$, with and without wave impingement with heated injection.

for the heated case at station 3 appears to be mixing quicker than the top of the unheated case potential core. This suggests that the 30% reduction in density in the slot has slightly boosted the density mixing. At station 4, both the unheated and heated density profiles are substantially mixed. The temperature effects of the slot have been diminished by station 4 so that the density gradient for the heated flow is not more than 10% larger than that of the unheated flow.

Some tests were run with an oblique shock impinging on the shear layer just upstream of station 4, which creates a strong streamwise pressure gradient affecting the mean flow data at station 4 in Fig. 10. The total temperature profile at station 4 with shock interaction exhibits no change across the adiabatic shock. As expected, the velocity profiles have lower values with shock impingement. The velocity jump across the shock was about equal for both the heated and unheated flows. The velocity profiles with the shock impingement, for both the heated and unheated cases, show no traces of the slot potential core. The shock impingement velocity profiles are very much like boundary-layer profiles. Thus, the adverse pressure gradient, created by the shock impingement, does increase the mixing.

The density profiles show larger values after the shock. The

density jump in the freestream is considerably greater than the density jump in the middle of the shear layer. The heated case density has a much smaller jump in the region of the slot flow.

Turbulent Intensity Measurements

Figures 11 and 12 are plots of turbulence intensities [$\overline{(\rho u)'^2}$ and $\overline{T_t'^2}$] expressed as percentages of the local mean values. Comparing heated and unheated case turbulence levels in Fig. 11, it appears that heating the flow had contradictory effects on the relative magnitudes of the mass flux turbulence. It increased this at stations 2 and 3 and slightly decreased it at station 4. Overall, heating the injectant appeared to increase the rms mass flux on average. The peak turbulence in the heated case profiles occurred lower in the shear layer than in the unheated cases, and this peak was highly correlated with the position of the temperature gradient. In contrast, the maximum mass flux turbulence in the unheated core profiles stayed in the upper middle of the shear layer between $y/H = 1.25$ and 1.5. At station 4, the turbulence peak had moved to within the injected region eliminating the remnants of the potential core.

Figure 12 shows total temperature fluctuation profiles, which have trends similar to those of the mass flux. In the case of unheated injection, the turbulence intensity, which is

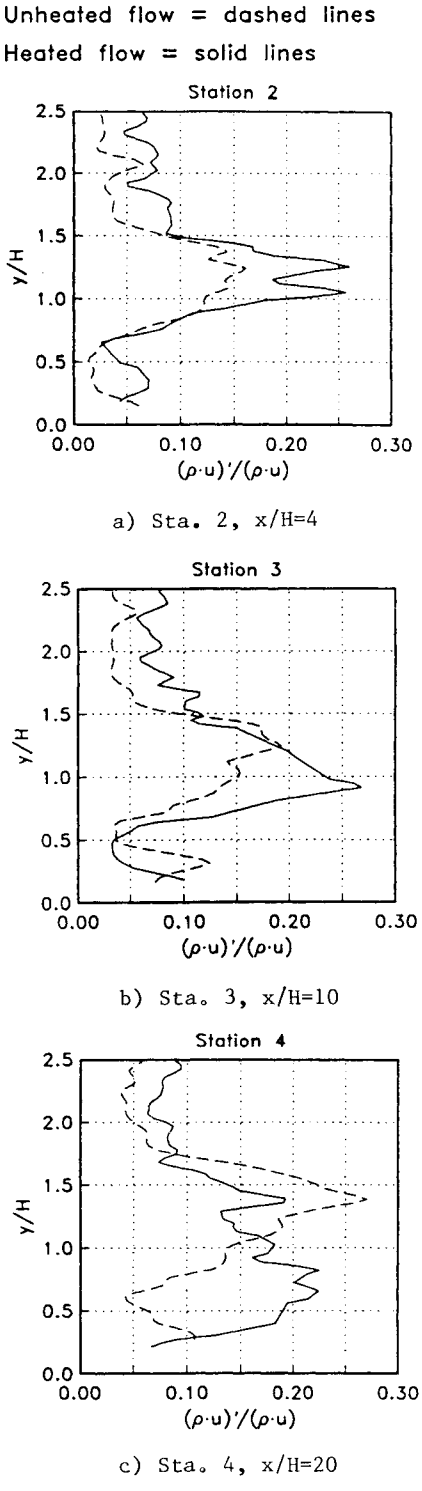

Fig. 11 Mass flux intensity profiles.

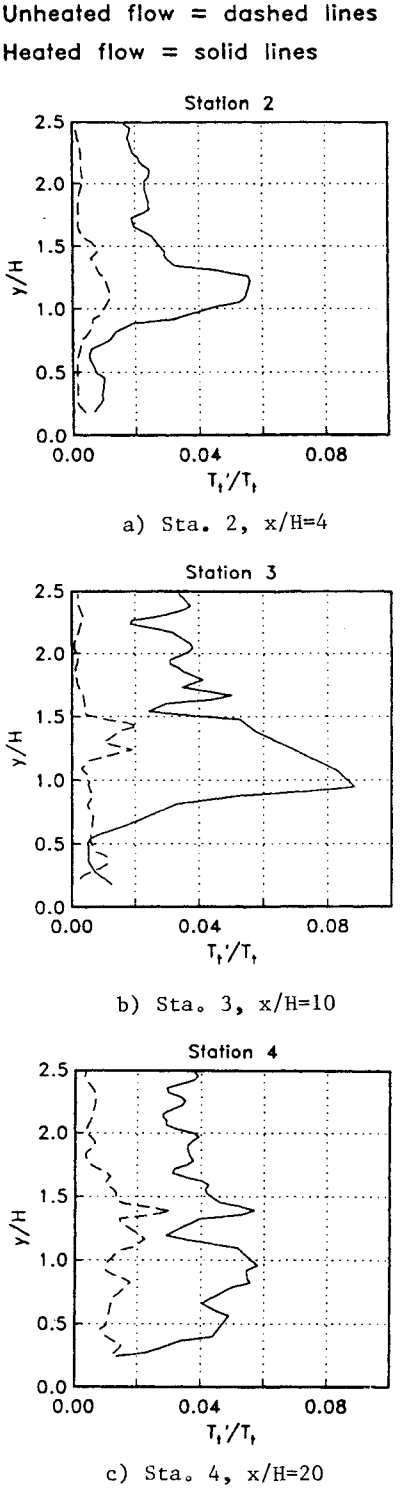

Fig. 12 Total temperature intensity profiles.

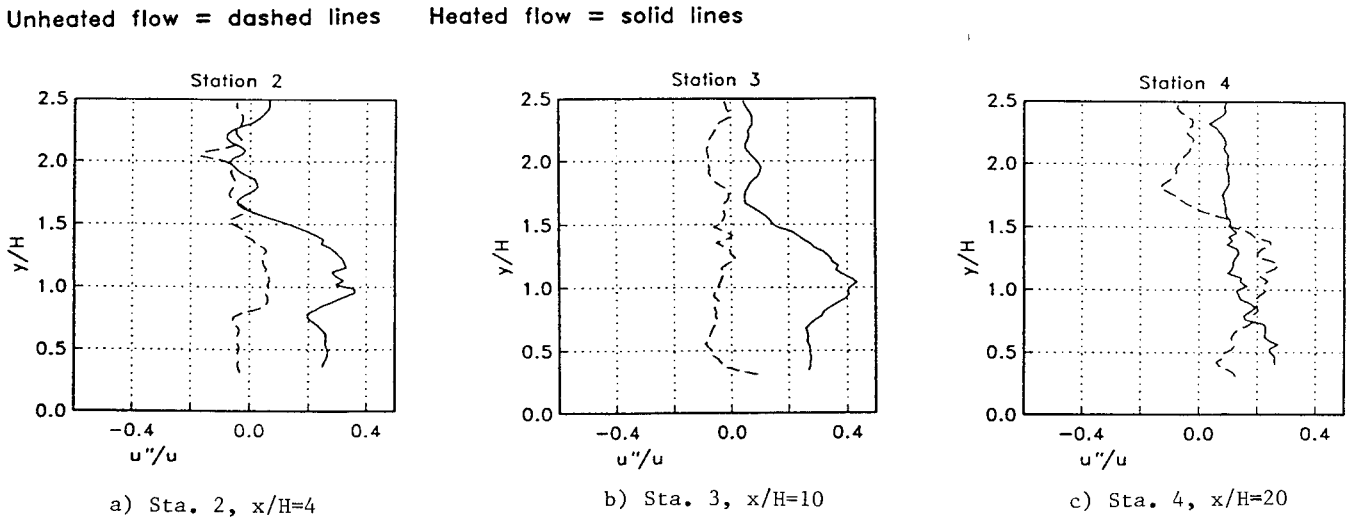

Fig. 13 Favre-averaged velocity intensity profiles.

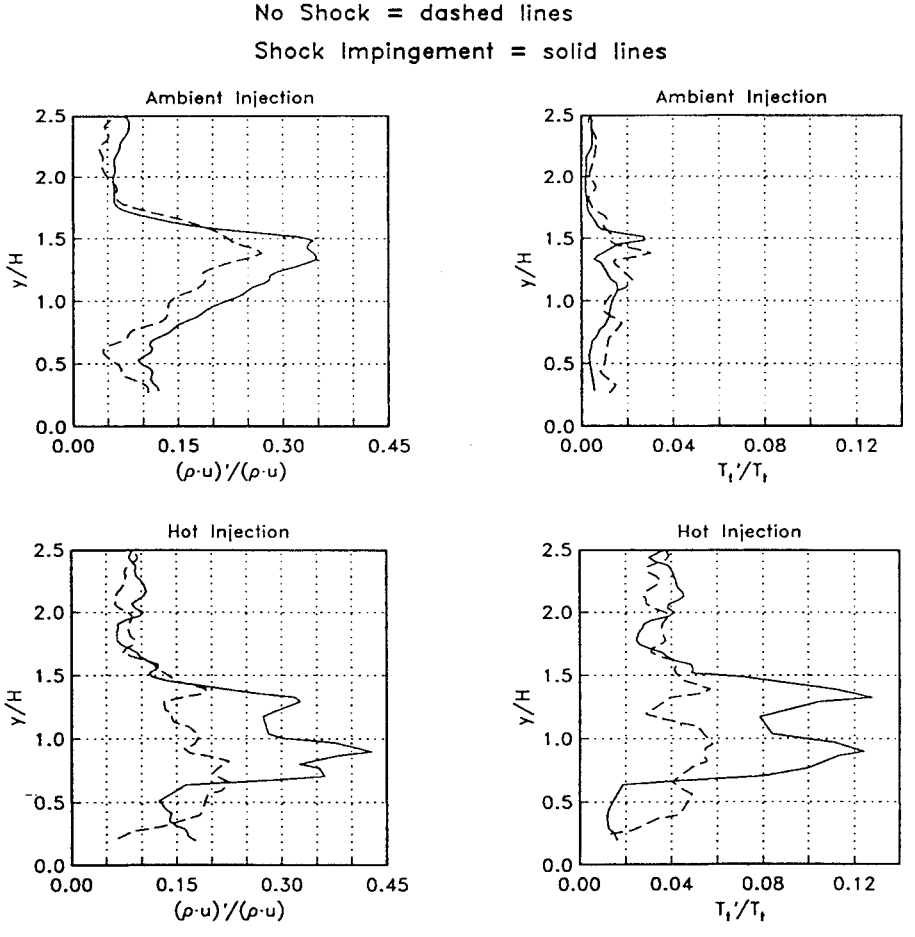

Fig. 14 Mass flux and total temperature intensity profiles at station 4, $x/H = 20$, with and without wave impingement.

much lower at almost all points than that in the heated injection flow, is nearly zero in the freestream and in the injectant core. This is expected because the mean total temperature is essentially uniform over the entire flow. In the heated flow, this turbulence was low near the wall, and it reached a peak at stations 2 and 3 during initial mixing of hot and cold pockets of gas. The turbulence is seen to drop somewhat while spreading across the layer at station 4, as seen earlier in the rms mass flux profiles.

The Favre-averaged velocity intensity $\overline{u''}$ is shown in Fig. 13. These data show that increasing the density variation by heating the injectant produces a clear increase in $\overline{u''}$, which is zero for small density variations. We are most confident of our turbulence data at stations 2 and 3.

Figure 14 shows the effect of shock impingement on total temperature and mass flux turbulence. In unheated injection, as expected, T_t' is unaffected by the shock. With heated injection, however, the large increase in T_t' indicates a large

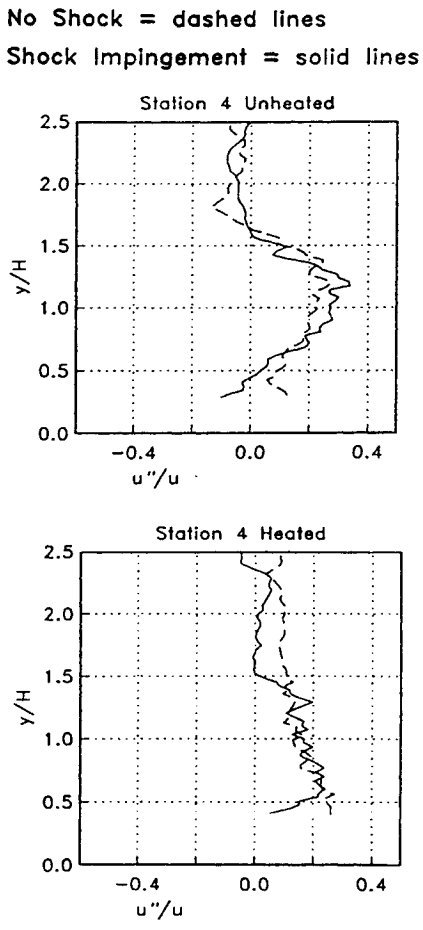

Fig. 15 Favre-averaged velocity intensity profiles at station 4, $x/H = 20$, with and without wave impingement.

amount of mixing of the warm and cool air streams. This agrees with the movement of hot air away from the wall seen in the mean profiles.

In the ambient injection case, the shock increased $(\rho u)'$ uniformly up to $y/H = 1.5$. In the heated injectant case, the turbulent mass flux rose in the lower shear layer under the influence of the shock, decreased in the remnant of the potential core, and increased close to the wall. The effect of the shock was to move mixing away from the wall, to increase the thickness of the lower boundary layer (as seen in the Schlieren), and to counteract the gradient-induced spreading of the mixing into the injectant. In contrast to the unshocked station 4 profiles, the turbulence was concentrated into a small band. The Favre-averaged velocity intensity shown in Fig. 15 was not greatly affected by the shock.

Conclusions

Detailed measurements of the flowfield have been taken for both heated and unheated supersonic slot injected flows. The flow profiles and the photographs describe the flowfield and are intended to provide useful data for understanding the flow and for comparison with numerical predictions. The velocity profiles in the unheated case tended to mix slightly faster than for the heated case; this was especially evident at station 3. The density field in the heated case tended to mix slightly faster than in the unheated case. Both sets of profiles agree that the main shear layer has merged with the wall boundary layer between stations 3 and 4, i.e., by $x/H = 20$. The schlieren pictures indicate merging by about $x/H = 12$ for the unheated case and $x/H = 20$ for the heated case.

Increasing the injectant temperature and thus decreasing the density by 30% does not appear to affect the spread of the mixing zone into the outer flow greatly. This did enhance the turbulent mixing in the lower region by involving a greater portion of that flow in the mixing process. This is reasonable since the large temperature and density gradients caused by heating the injectant are below most of the shear layer. Interestingly, increased turbulence occurs despite the lower mean velocity gradient caused by heating the injectant. Although the maximum mass flux turbulence levels were not greatly affected by heating the injectant, mixing was enhanced in the slot flow by station 4, and the turbulence scale in the pictures increased substantially.

It was possible to deduce values of the Favre-averaged velocity intensity $\overline{u''}$ by combining the hot-wire and mean-probe results with the aid of some rational, but not rigorously justified, assumptions. The results show that the larger density variations produced by heating the injectant increased the levels of this quantity. There is little data in the literature for $\overline{u''}$ to compare with our measurements. Some data taken in a low-speed propane jet in air by Schefer, Dibble, and Hartmann at Sandia using optical methods show $\overline{u''}/\Delta\tilde{u}$ of about 0.3, which is the same order as obtained here.

The effect of a strong streamwise pressure gradient on the fully developed wall/shear layer by shock impingement was examined. Although the shear layer did not change greatly in appearance, the shock impingement did strongly affect the mean-flow profiles. The shock impingement both added turbulence to the flow and augmented mixing in the layer. In general, shock interaction increased the level of turbulence and thickened the shear layer. Interestingly, the shock had little effect on the Favre-averaged intensity, $\overline{u''}$.

With the $\bar{\rho}$ and $\bar{u}$ profiles available, it was possible to integrate the mass flux $(\bar{\rho}\bar{u})$ profiles across the viscous region at the last station in an attempt to deduce entrainment rates between the injection station and the last station. The entrainment rates so calculated were in agreement with the well-known Crocco-Lees relation $d\dot{m}/dx = C\rho_\infty u_\infty$ if $C \approx 0.015$, which is in the range of usual findings. Within the uncertainties of these calculations, no signficant difference in entrainment rates up to $x/H = 20$ for the heated and unheated injection cases was found.

Acknowledgments

The support for this work by the Applied Physics Laboratory of the Johns Hopkins University, Contract Monitor Harold E. Gilreath, is gratefully acknowledged.

References

[1]Visich, M., Jr., and Libby, P. A., "Experimental Investigation of Mixing of Mach Number 3.95 Stream in Presence of Wall," NASA TN-D-247, Feb. 1960.

[2]McRee, D. I., Peterson, J. B., and Braslaw, A. L., "Effect of Air Injection Through a Porous Surface and Through Slots on Turbulent Skin Friction at Mach 3," NASA TN-D-2427, Aug. 1964.

[3]Goldstein, R. J., Eckert, E. R. G., Tsou, R. K., and Haji-Sheikh, A., "Film Cooling with Air and Helium Injection through a Rearward-Facing Slot into a Supersonic Air Flow," *AIAA Journal*, Vol. 4, No. 6, 1966, pp. 981–985.

[4]Peake, D. J., "The Use of Air Injection to Prevent Separation of the Turbulent Boundary Layer in Supersonic Flow," British Ministry of Aviation, Aeronautical Research Council CP No. 890 (N67-21194), London, 1966.

[5]Peterson, J. B. Jr., McRee, D. I., Adcock, J. B., and Braslow, A. L., "Further Investigation of Effect of Air Injection Through Slots and Porous Surfaces on Flat-Plate Turbulent Skin Friction at Mach 3," NASA TN-D-3311, N66-20928, March 1966.

[6]Howell, G. A., and Tatro, R. E., "Tangential Fluid Injection for Control of Shock-Boundary Layer Interaction," AIAA Paper 66-656, June 1966.

[7]Schetz, J. A., and Gilreath, H. E., "Tangential Slot Injection in Supersonic Flow," *AIAA Journal*, Vol. 5, No. 12, 1967, pp. 2149–2154.

[8]Gilreath, H. E., and Schetz, J. A., "Transition and Mixing in the

Shear Layer Produced by Tangential Injection in Supersonic Flow," American Society of Mechanical Engineers Paper 71-FE-24, New York, Feb. 1971.

[9]Carey, A. M., and Hefner, J. N., "Film-Cooling Effectiveness and Skin Friction in Hypersonic Turbulent Flow," *AIAA Journal*, Vol. 10, No. 9, Sept. 1972.

[10]Schetz, J. A., and VanOvereem, J., "Skin Friction Reduction by Injection Through Combinations of Slots and Porous Sections," *AIAA Journal*, Vol. 13, No. 8, Aug. 1975, pp. 971–972.

[11]Waltrup, P. J., and Schetz, J. A., "Tangential Slot Injection of Carbon Dioxide and Helium into a Supersonic Air Stream," American Society of Mechanical Engineers Paper 72-WA/FE-37, New York, July 1972.

[12]Kenworthy, M., and Schetz, J. A., "An Experimental Study of Slot Injection into a Supersonic Stream," NASA CR-2128, Jan. 1973.

[13]Walker, D. A., Campbell, R. L., and Schetz, J. A., "Turbulence Measurements for Slot Injection in Supersonic Flow," AIAA Paper 88-0123, 1988.

[14]Pike, E. R., "The Applications of Photon-Correlation Spectroscopy to Laser Doppler Velocimetry," *The Use of the Laser Doppler Velocimeter for Flow Measurements*, proceedings of a Project SQUID Workshop, Purdue Univ., West Lafayette, IN, March 1972, pp. 133–146.

[15]Yanta, W. J., "Use of the LDV in Subsonic and Supersonic Flow," *The Use of the Laser Doppler Velocimeter for Flow Measurements*, proceedings of a Project SQUID Workshop, Purdue Univ., West Lafayette, IN, March 1972, pp. 324–349.

[16]Kovasznay, L. S. G., "The Hot-Wire Anemometer in Supersonic Flow," *Journal of Aeronautical Sciences*, Vol. 17, No. 9, 1950, pp. 565–594.

[17]Morkovin, M., "Fluctuations and Hot-Wire Anemometry in Compressible Flow," AGARD 24, Paris, 1956.

[18]Kovasznay, L. S. G., "Turbulence in Supersonic Flow," *Journal of Aeronautical Sciences*, Vol. 20, No. 10, 1953, pp. 657–674.

[19]Walker, D. A., Ng., W. F., and Walker, M. D., "Experimental Comparison of Two Hot-Wire Techniques for Resolution of Turbulent Mass Flux and Local Stagnation Temperature in Supersonic Flow," *AIAA Journal*, Vol. 26, No. 3, 1989.